

SUBMITTED AUG 28, 2002

Preprint typeset using L^AT_EX style emulateapj v. 14/09/00MEASURING CLUSTER PECULIAR VELOCITIES AND TEMPERATURES AT CM AND MM
WAVELENGTHS

GILBERT P. HOLDER

School of Natural Sciences, Institute for Advanced Study, Princeton NJ 08540

holder@ias.edu

submitted Aug 28, 2002

ABSTRACT

We present a detailed investigation of issues related to the measurement of peculiar velocities and temperatures using Sunyaev-Zel'dovich (SZ) effects. We estimate the accuracy to which peculiar velocities and gas temperatures of distant galaxy clusters could be measured. With μK sensitivity on arcminute scales at several frequencies it will be possible to measure peculiar velocities to an accuracy of $\sim 130 \text{ km s}^{-1}$ and gas temperatures to better than 1 keV. The limiting factor for the accuracy of v_{pec} is the presence of bulk motions within the galaxy cluster, even for apparently relaxed clusters. The accuracy of the temperature is mainly limited by noise. These results are independent of redshift. Such constraints can best be achieved with only three frequencies: one in the Rayleigh-Jeans region ($\nu < 40 \text{ GHz}$), one near 150 GHz, and the third at 300 GHz or higher. Measurements at the null of the thermal SZ effect are of marginal utility, other than as a foreground/background monitor.

Subject headings: cosmology: theory — large-scale structure of the universe — cosmic microwave background — galaxies: clusters: general

1. INTRODUCTION

Observations of the Sunyaev-Zel'dovich (SZ) effect (Sunyaev and Zel'dovich 1972) are currently at a mature stage. Highly significant detections are now routine and the next generation of instruments is about to exploit the SZ effect to provide deep surveys of galaxy clusters (for a recent review see Carlstrom *et al.* 2002). All current and near-future instruments are devoted to studies of the *thermal* SZ effect. There are a host of yet more subtle distortions of the cosmic microwave background (CMB) spectrum that contain a wealth of information related to the cluster's peculiar velocity (v_{pec}) and the gas temperature (T) of the intracluster medium.

In this paper we investigate the most significant of the subtler distortions, namely those due to the line-of-sight motion (the kinetic SZ effect) and the distortion of the spectrum due to relativistic effects (the relativistic thermal SZ effect). These effects are discussed in several reviews (Rephaeli 1995; Birkshaw 1999) and are presented in great detail by several authors (Sunyaev and Zel'dovich 1980; Rephaeli 1995; Challinor and Lasenby 1998; Sazonov and Sunyaev 1998; Itoh, Kohyama, and Nozawa 1998; Nozawa, Itoh, and Kohyama 1998; Molnar and Birkshaw 1999; Dolgov, A. D. *et al.* 2001).

At sensitivities below $\sim 1 \mu K$ some higher order effects could be important such as multiple scatterings and transverse velocities. At such low levels, CMB anisotropies will be also be a very difficult contaminant. For simplicity, we restrict ourselves to the most significant effects.

The importance of using the SZ effect to its fullest potential comes from its redshift independence. As a spectral distortion of the CMB, it redshifts along with the CMB and the amplitude of the distortion does not suffer from cosmological dimming. If there are clusters at redshift $z \sim 2$ (as there should be in standard models of structure formation) they will be very faint in X-rays, and perhaps undetectable if the gas has been preheated by an early burst of star formation. An independent probe of the gas temperature would be invaluable, and preliminary steps along these lines are being made (Hansen, Pastor, & Semikoz 2002). Measurements of peculiar velocities would allow recon-

struction of the large scale density field on scales comparable to the horizon (Dore, Knox, and Peel 2002). A firm understanding of the large scale density inhomogeneities would allow new tests of galaxy formation and provide a view of the evolution of structure.

In the next section we lay out the physical effects which allow such powerful tests. In §3 we investigate the observing frequencies which are best suited for such an investigation. The details of the simulations and map-making methods are outlined in §4 and results are presented in §5. We close with a discussion of practical issues and a summary.

2. SZ EFFECTS

CMB photons have roughly a 1% probability of interacting with free electrons in the deep potential wells of galaxy clusters. Compton scattering leads to an exchange of energy between the cool photons and hot electrons, causing a distortion of the CMB spectrum. This is known as the thermal SZ effect. Both the cross-section for scattering and the electron energy distribution depend on the electron gas temperature, providing a means of probing the gas temperature. The general form of the thermal SZ effect is a temperature decrement at low frequencies and an increment at high frequencies. The main effects of the gas temperature are to slightly reduce the amplitude of the distortion (in a frequency dependent way) and to shift the null of the distortion to a slightly higher frequency.

The kinetic SZ effect arises from a bulk velocity of the galaxy cluster along the line of sight. The scattered CMB photons essentially pick up a slight redshift or blueshift from the peculiar velocity of the cluster. The imprint on the CMB is a purely thermal distortion, i.e., the spectrum is exactly that of a blackbody at a slightly higher or lower temperature.

All of these effects are very small. The typical energy exchange per scattering for the thermal SZ effect is only $\sim 1\%$ (i.e., $kT/m_e c^2$) and only 1% of photons, on average, undergo scattering. Therefore, the cumulative effect relative to the 2.73 K background is on the order of one part in 10^4 . The kinetic effect is even smaller, since v_{pec}/c is typically on the order of

10^{-3} , making the typical fractional energy exchange an order of magnitude below that expected for the thermal effect. The distortions of the thermal SZ effect due to the gas temperature are comparable in magnitude to the kinetic SZ effect. Importantly, all of these effects have different spectral behavior, manifesting themselves differently as a function of frequency. Figure 1 shows some SZ effects as a function of frequency, both for temperature and intensity. The dominant effect is clearly the non-relativistic thermal SZ effect, showing the well-known decrement at low frequencies and increment at higher frequencies. Note that the optical depth for the lower temperature cluster has been scaled to provide the same net Comptonization. Both peculiar velocity and the gas temperature shift the spectrum, but the effect of the velocity on the temperature is constant with frequency, while the gas temperature provides a non-trivial spectral signature. This could allow a well-designed experiment with several observing frequencies to separate these effects and measure the gas temperature and peculiar velocity.

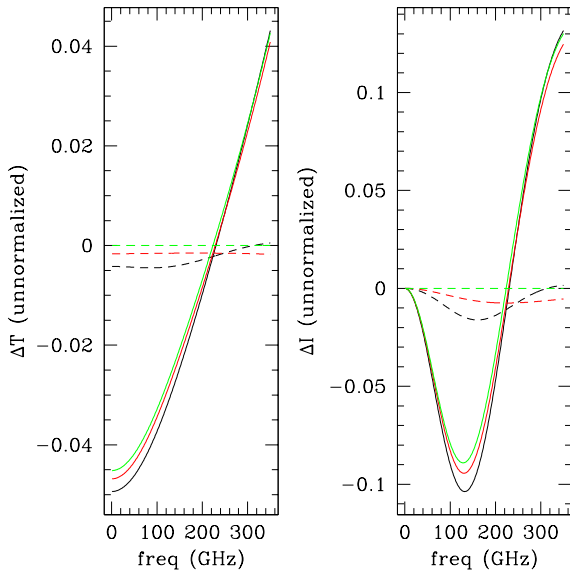


FIG. 1.— Effects of relativistic corrections and peculiar velocities to SZ spectrum. Black curves show $(T_e/\text{keV}, v/(\text{km/s}), \tau) = (6, -500, 0.02)$, red curves show $(12, -500, 0.01)$, green shows $(12, 0, 0.01)$. Dashed curves show all curves relative to $(12, 0, 0.01)$.

3. OBSERVING FREQUENCIES

Separation of the various SZ components requires at least three observing frequencies (there are three unknowns: τ, T, v). To address the best positioning of these frequencies, a small numerical experiment was performed.

We take the range of observable frequencies to be 10-350 GHz, with lower frequencies likely contaminated by radio point sources and higher frequencies possibly contaminated by galactic dust and extragalactic dusty galaxies. In steps of 10 GHz, we assumed the first frequency was at a frequency in the range 10-300 GHz. For each of these values, we then stepped ν_2 in 10 GHz intervals over all frequencies from $\nu_1 + 10$ to 330 GHz, and then allowed the third frequency ν_3 to be in the range $\nu_2 + 10$ to 350 GHz.

At each position we use the fitting functions of Nozawa, Itoh, and Kohyama (1998) to calculate the expected SZ temperature decrement or increment. We use the Fisher matrix formalism to estimate errors in the three parameters for each (ν_1, ν_2, ν_3)

point. This method essentially approximates the likelihood function \mathcal{L} as a Gaussian function of parameters \vec{p} near its peak and assumes that the curvature (second derivative) at the peak gives a good estimate of uncertainties.

We define the Fisher matrix as

$$F_{ij} = \langle \frac{d^2 \ln \mathcal{L}}{dp_i dp_j} \rangle , \quad (1)$$

where the angled brackets indicate an ensemble average over all realizations of data. If the data products are taken to be $\Delta T_{\nu\alpha}$, the temperature decrements or increments at frequencies $\nu = \nu_\alpha$, then the likelihood of the parameters for a given set of data is simply

$$-2 \ln \mathcal{L} = \chi^2 = \sum_{\alpha=1}^3 \frac{[\Delta T_{\nu\alpha} - \Delta \bar{T}(\nu_\alpha, \vec{p})]^2}{\sigma_\alpha^2} , \quad (2)$$

where $\Delta \bar{T}$ is simply the model prediction as a function of frequency and fiducial model.

In this case, the Fisher matrix reduces to (after ensemble averaging)

$$F_{ij} = \sum_{\alpha=1}^3 \frac{1}{\sigma_\alpha^2} \frac{d \Delta \bar{T}}{dp_i}(\nu_\alpha, \vec{p}) \frac{d \Delta \bar{T}}{dp_j}(\nu_\alpha, \vec{p}) , \quad (3)$$

where all derivatives are evaluated at the point where the \vec{p} take their fiducial values.

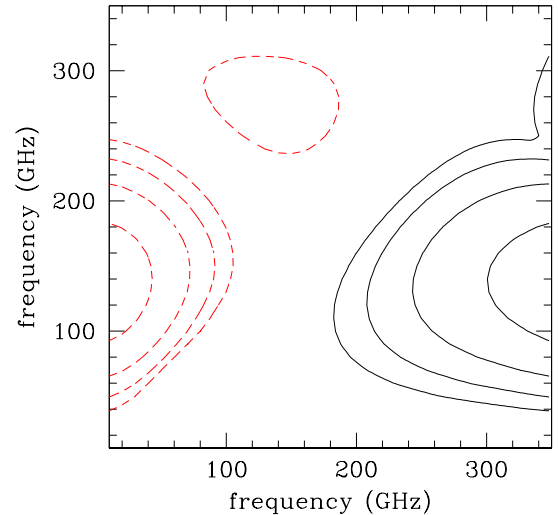


FIG. 2.— Uncertainty volumes as a function of observing frequencies. Red dashed contours show size of uncertainty volume for ν_1 on x-axis and ν_2 on y-axis, while black contours instead are for ν_3 on the x-axis. Contours are in steps of 0.2 dex relative to smallest volume. Fiducial model in this case has $T_e = 12 \text{ keV}$, $v = 200 \text{ km/s}$, $\tau = 0.01$.

Derivatives are calculated numerically by stepping from the fiducial model by $\pm 0.1 \text{ keV}$ in temperature, $\pm 10 \text{ km/s}$ in velocity and $\pm 5\%$ of the fiducial τ . The one sigma single parameter uncertainties, marginalized over other parameters are then simply $(F^{-1})_{ii}$. Note that a Gaussian prior in a parameter is easily applied by simply adding $1/\sigma_i^2$ to the diagonal element F_{ii} , where σ_i^2 is the variance of the prior on parameter i .

In figure 2 we show the square root of the determinant of the inverse Fisher matrix as a function of frequencies, assuming equal variances at each point of $\sigma_\alpha = 1 \mu K$. The square root of the determinant of the inverse Fisher matrix is a measure of the

volume of the ellipsoid in parameter space that would give the single-parameter 68% confidence regions. For uncorrelated parameters, the determinant would simply be $\prod_{i=1}^3 \sigma_i^2$, where σ_i^2 is the variance in parameter i .

The best results are obtained if the first frequency is as low as possible and the third frequency is as high as possible. For practical purposes, all frequencies below about 90 GHz work well, as do all frequencies above 300 GHz. What is interesting is that the second frequency is best placed at 150 GHz, not at the null of the thermal effect. Frequencies near the null of the thermal effect (~ 220 GHz) are not particularly good places to try to get constraints on parameters. Furthermore, higher order terms to the observed spectrum can become significant near the null, complicating the analysis.

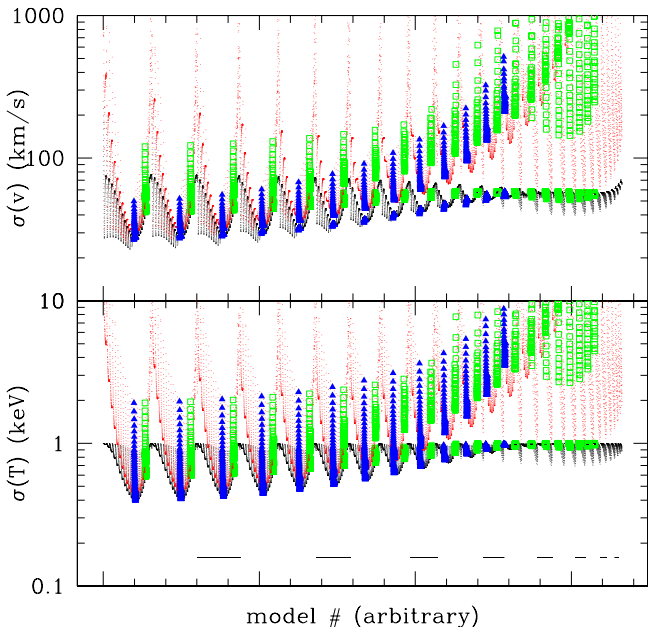


FIG. 3.— Possible measurement uncertainties for fiducial $1 \mu\text{K}$ sensitivity experiment for different frequency coverages and an assumed fiducial model of $T_e=6 \text{ keV}$, $v=200 \text{ km/s}$, $\tau=0.01$. Each model on the x-axis is a triplet of frequencies (ν_1, ν_2, ν_3) , such that ν_1 increases from 10 GHz at the left to 270 GHz at the right (non-linearly). At each ν_1 the other possible frequencies are similarly systematically checked. Red points are from SZ data alone while black points show effect of a $\pm 1 \text{ keV}$ independent measure of the gas temperature. Horizontal lines in bottom panel indicate models with $\nu_1=30-240 \text{ GHz}$ in steps of 30 GHz, i.e., every third step in ν_1 . Open squares (green) indicate models with $\nu_2=220 \text{ GHz}$ while solid triangles (blue) show models with $\nu_2=150 \text{ GHz}$.

As a concrete example of why the thermal null is not necessarily a good place, take frequencies of 150, 220, 300 GHz. In this case, the main effect of the temperature corrections is to reduce the thermal SZ spectrum at the two end frequencies, and to shift the thermal SZ null to a slightly higher frequency. Without an external temperature measurement, this can be degenerate with a slightly lower Comptonization ($\tau[kT/m_ec^2]$), which reduces the overall amplitude of the curve, and a peculiar velocity away from the observer, which slightly shifts the curve toward lower temperature decrements/increments. Whether or not this degeneracy can be broken will depend somewhat on the fiducial model.

Note that we have assumed uniform errors at each frequency in *temperature* difference measurements (not intensity). This is highly idealized, in that foregrounds and noise are highly

frequency-dependent. As motivation for this choice, we assume that this sort of experiment would be a natural outgrowth of a small-angle CMB experiment, where it might be expected that the experimental goal would be something close to uniform temperature sensitivity as a function of frequency. We have also ignored finite bandwidth issues, which could be especially problematic at the null of the thermal effect but should not be a large problem at the frequencies which turn out to be optimal.

If one has gas temperatures from X-ray spectroscopy, the constraints on parameters might be expected to improve significantly. We added a term to the Fisher matrix corresponding to an independent gas temperature measurement of $\pm 1 \text{ keV}$. As shown in figure 3 this does not significantly change the preferred frequency placement, as can be seen by the lowest variances coinciding either with or without external gas temperature information. Furthermore, at a sensitivity of $1 \mu\text{K}$ the gas temperature measurement from the SZ data alone will be sufficiently good that a $\pm 1 \text{ keV}$ measurement is not of much additional use at frequencies which are nearly optimal. For non-optimal frequency coverage, the additional information on the gas temperature provides tremendous leverage for velocity information. From hydrodynamical simulations, it would not be expected that the X-ray emission weighted temperature will agree with the mean electron temperature (which is relevant here) to better than 1 keV (Mathiesen and Evrard 2001).

From the Fisher matrix estimates, single parameter uncertainties on gas temperature, peculiar velocity, and optical depth, assuming a noise level of $1 \mu\text{K}$ per frequency, are $\delta T \sim 0.5 \text{ keV}$, $\delta v \sim 30 \text{ km s}^{-1}$ and $\delta \tau \sim 6 \times 10^{-4}$ for a fiducial model of $T=6 \text{ keV}$, $v_{pec}=200 \text{ km s}^{-1}$, $\tau = 0.01$. These results will scale inversely with the assumed value of τ and will scale linearly with the assumed noise level.

4. SIMULATIONS

For an isothermal galaxy cluster with a unique peculiar velocity, the results of the previous section are sufficient to estimate uncertainties. In reality, however, galaxy clusters are not isothermal and bulk flows on the order of the sound speed can persist for up to 10% of the Hubble time. In order to investigate the effects of such phenomena we turn to numerical simulations of galaxy clusters.

The simulations that we use have been described elsewhere (Holder *et al.* 2000; Mohr, Mathiesen, and Evrard 1999; Mohr and Evrard 1997). The cosmological model was a flat low density universe with matter density (in units of the critical density) of 0.3 and a Hubble constant of $80 \text{ km s}^{-1} \text{Mpc}^{-1}$. The simulation method is $\text{P}^3\text{M-SPH}$ (Evrard 1988), where the hydrodynamics are done using the SPH method and the gravity is done with a particle-particle method for nearby particles and long-range forces are calculated from a grid. A dark matter only simulation was performed in a large volume to identify the positions of galaxy clusters, and all particles that ended up within the cluster virial radius were traced back to the initial conditions and replaced with more particles, some dark matter and some gas, each of smaller mass. Large particles outside the virial radius acted to include the effects of large scale tidal fields. The net momentum of the simulation volume for each galaxy cluster was zero.

Each gas particle in an SPH scheme has a smoothing radius that roughly corresponds to the mean distance to its N th nearest neighbor, where N is about 24. We made projected

maps of the relevant properties of the gas distribution (optical depth, average velocity, gas temperature, mean Comptonization, SZ effects) along the three principal axes of the simulation by spreading the electrons associated with each gas particle uniformly within a disk of radius equal to roughly one third the SPH smoothing length. While this had the desirable effect of making the maps smoother (visually) by reducing shot noise, the quantitative effects of the smoothing kernel were negligible.

Three clusters were selected from the $z = 0.5$ outputs of the simulations, as the three most massive clusters in the simulation set at that redshift. For each particle in the simulation, the gas temperature was used to estimate its SZ effect contribution to the projected map, again using the fitting functions of Nozawa, Itoh, and Kohyama (1998). By adding up the contribution of each particle we made synthetic SZ maps of each galaxy cluster, including the effects of relativistic corrections and peculiar velocities. The resulting maps had a resolution of $25''$. The results are not sensitive to the resolution of the maps in that higher resolution did not have any discernible effects. This angular resolution also approximately corresponded to the spatial resolution of the simulation.

At each point in the maps we used the SZ maps and the Fisher matrix methods of the previous section to calculate the expected measurement accuracy that would be possible in a high resolution, sensitive experiment. An angular diameter distance of 1000 Mpc was assumed.

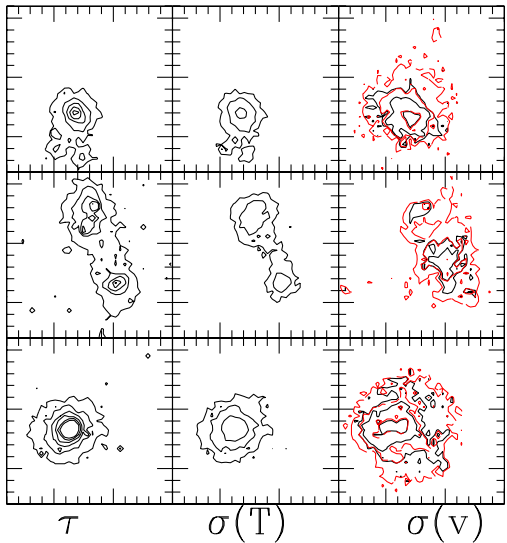


FIG. 4.—Surface maps of simulated galaxy clusters. From top to bottom are three different simulated clusters. From left to right columns show maps of optical depth, possible measurement accuracies on gas temperature and peculiar velocity. The maps are $14''$ on a side, with each tickmark showing $1'$. Contour levels in left panels are at multiples of 2×10^{-3} , in center panels correspond to 0.5, 1, 2 keV and in right panel show 20, 50, 100 km/s. Red dashed line in right panels correspond to measurement uncertainty in velocities assuming an independent measurement of the gas temperature of ± 1 keV.

5. RESULTS

As might be expected, the most important determinant of success in parameter measurement is the optical depth, as shown in the simulation maps in figure 4. All of the uncertainties trace the optical depth map fairly well. In all clusters, within the central few arcminutes the gas temperature can be

measured to better than 1 keV and the velocity to better than 100 km/s. Introducing external gas temperature information improves the size of the region over which reliable velocity measurements are possible to roughly $7'$.

The velocity uncertainty maps are much more ragged than the gas temperature uncertainty maps. This is mainly due to “lumpiness” in the projected velocity and gas temperature maps. In many ways, the velocity is the most difficult quantity to measure, because it relies on a good measure of the optical depth, which in turn rests on a reliable gas temperature measurement. Being at the “end of the line” leads to increased sensitivity to small scale inhomogeneities.

Such accurate measures of the bulk velocity over scales of several arcminutes will in reality be virtually impossible. While the gas temperature has a unique spectral signature, the effects of the bulk velocity have a spectral signature that is identical to the intrinsic primary and secondary anisotropies in the CMB. Most of the CMB anisotropy power is on much larger angular scales, but it is instructive to estimate the region over which one could best measure the bulk velocity.

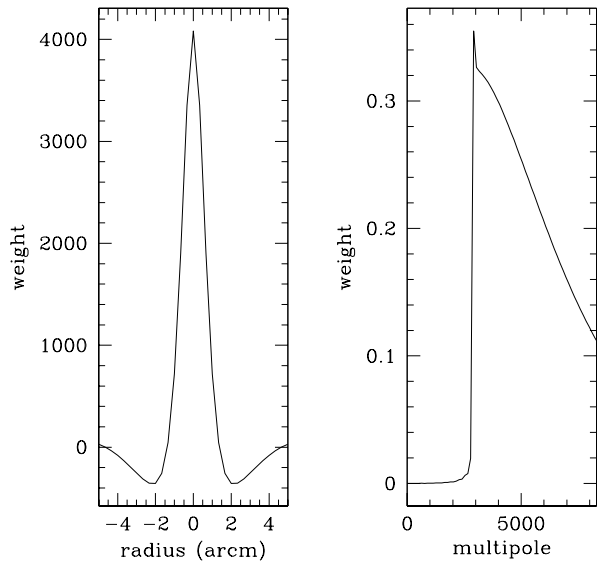


FIG. 5.—Filters necessary to remove noise from CMB primary and secondary anisotropies in real space (left) and in Fourier space (right). The normalization is unimportant in this figure.

The tools for such an analysis are laid out in Haehnelt and Tegmark (1996). As an update to their work, we investigate smaller scales and lower noise levels, appropriate for the next generation of small-angle CMB experiments. We calculate the primary CMB anisotropies using the publicly available CMB-Fast code (Seljak and Zaldarriaga 1996), and assume secondary anisotropies are well described by flat band power and an rms temperature anisotropy of $1 \mu K$, and also assume thermal noise of $1 \mu K$ in $1'$ pixels, although we ignore beam effects. As a model for the optical depth, to be conservative we assume that the gas follows the 3D density profile $\rho \propto [1 + (r/r_c)^2]^{-1}$ with $r_c = 45''$ (expressed as an angle) and an isothermal gas. Clusters are almost certainly much more compact than this. The optimal filter for such a profile is shown in figure 5. The Fourier space version is shown with spatial wavenumbers expressed in units of multipoles, assuming a flat-sky approximation. To convert to the usual $u-v$ plane of interferometry, $\ell = 2\pi R_{uv}$, where R_{uv} is

the radius in the $u-v$ plane. As can be seen in the Fourier space profile, it is effectively a simple high-pass filter that removes the large amount of power on large scales. From the real space version, it can be seen that effectively all power beyond a radius of 2' is filtered, with a FWHM of roughly 2'. The particulars of the cluster model are essentially irrelevant, mainly affecting the exact shape of the high ℓ taper and only modestly affecting the FWHM of the filter. An excellent discussion of filtering issues is presented in Haehnelt and Tegmark (1996).

What can be concluded from figure 5 is that peculiar velocity measurements of galaxy clusters can only be performed in the inner two to four arcminutes because of severe contamination by CMB anisotropy. Because only a relatively small portion of the cluster is accessible for observations, bulk velocities within the cluster, due to somewhat recent mergers can be a large source of confusion. Bulk flows moving at roughly the sound speed (roughly 1000 km/s) containing ten percent of the mass would be expected to mimic a signal of the entire cluster moving at 100 km/s. This is not a particularly unlikely occurrence, as a 10:1 mass ratio merger should happen quite regularly. These bulk flows should remain intact for a few crossing times. For a 1000 km/s flow crossing 1 Mpc, the crossing time is roughly 1 Gyr.

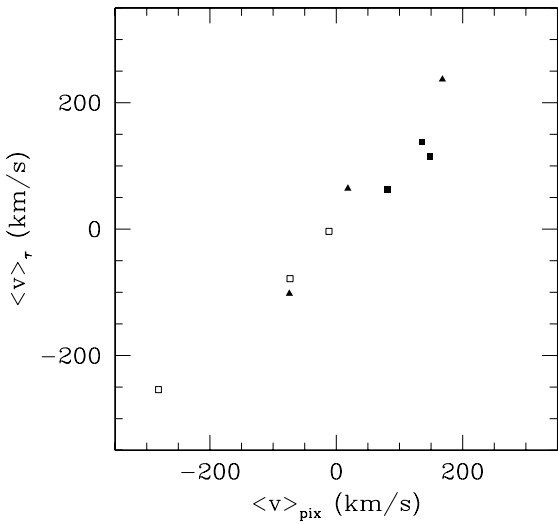


FIG. 6.— Comparison of average velocity in central 2' derived from averaging the pixel values of the velocities vs averaging the pixels weighted by the optical depth. Each simulated cluster has a different symbol, and three projections of each cluster are shown (x,y,z). From top to bottom in figure 4: open squares, solid triangles, solid squares.

In figure 6 we show two measures of the effects of bulk flows on peculiar velocity measurements using the simulated galaxy clusters. We calculated the average velocity within the central two arcminutes of three projections of the three simulated clusters. This was done either as an average of the individual pixels, or as an optical depth weighted average of the pixels. A top-hat window was assumed, rather than the optimal filter discussed above. For the simulation that is clearly a merging system, the velocities were separately calculated for the central regions of each clump and then averaged. The individual clumps for the merger event had individual velocities of ~ 500 km/s in opposite directions. It would be readily apparent from the thermal SZ map that this cluster is a double in the process of merging

and it would be straightforward to take this into account. This should be a good estimate of the typical errors that would be incurred due to bulk flows within the intracluster medium. The dark matter in the simulation has no net momentum, so a perfect reflection of the bulk velocity would be no net velocities.

From figure 6, it is apparent that there is significant confusion coming from internal bulk flows. The *rms* velocities from these three simulations are 135 km/s for the pixel-averaged velocity and 141 km/s for the optical depth weighted average velocity. While it may be possible to reduce this confusion somewhat, and more simulations are required to quantify this more precisely, it is clear that measurements of peculiar velocities to an accuracy better than 100 km/s will be very difficult. This is in agreement with Haehnelt and Tegmark (1996), who found that bulk motions within a simulated galaxy cluster led to a $\sim 10\%$ mis-estimate of the input 1000 km/s peculiar velocity, suggesting that the bulk flows are contributing ~ 100 km/s uncertainties. This has also been found independently by Nagai, Kravtsov, and Kosowsky (2002).

Because individual measurements will not be noise-limited, it may turn out to be better to use the distribution of velocities rather than velocities weighted by optical depth, in the same way optical studies use galaxy velocity distributions to estimate the mean redshift. The coherence length of the bulk flows are unfortunately not much smaller than a few arcminutes, so it is not clear how much is gained.

6. DISCUSSION AND CONCLUSIONS

Measurements of peculiar velocities of galaxy clusters at microwave frequencies will soon be possible. We have shown that multi-frequency, sensitive observations could measure peculiar velocities to an accuracy of roughly 100 km/s. Measurements of gas temperatures will be useful, with uncertainties possibly smaller than could be achieved with X-ray spectroscopy. The redshift independence of the SZ effect will make this an extremely powerful tool for studies of distant clusters. Exploring differences between X-ray emission weighted and SZ emission weighted temperature maps will no doubt be interesting.

Foregrounds and backgrounds will be important barriers to such precise studies of peculiar velocities. The primary anisotropies of the CMB will become problematic on scales larger than a few arcminutes, and point source removal will be very difficult. It has not yet been demonstrated that the atmosphere will not be a problem for ground-based experiments, but there is no *a priori* evidence that there will be a problem. Inter-frequency calibration to the requisite precision will be a significant technical challenge.

Point sources come in (at least) two varieties. At frequencies below ~ 90 GHz point sources (primarily extragalactic AGN but also star-forming galaxies) have historically been a problem for SZ measurements and they are unlikely to go away. The best solution seems to be simultaneous monitoring at extremely high (a few arcseconds) resolution. At higher frequencies, dusty star-forming galaxies are ubiquitous. If no source subtraction is done, confusion could easily be at the level of $10 \mu K$, comparable to the kinetic SZ signal (Blain 1998). Currently very little is known about these sources, making spectral subtraction (measuring at a higher frequency where the SZ signal is negligible) difficult; the ultimate solution may require something like ALMA to remove the point sources at mm wavelengths. There is no evidence for variability in these sources, so it will not be necessary to do the subtraction si-

multaneously, as is required for the occasionally variable radio point sources.

The best frequencies for observation turn out to not include the null of the thermal SZ effect. The best strategy is to have a Rayleigh- Jeans band (below 90 GHz), a high frequency band (above 300 GHz) and a band near 150 GHz. Much has been made of the null of the thermal SZ effect, and it will be important as a check for systematic errors, but it is not a good frequency for cluster studies.

Bulk velocities within the cluster, combined with contamination from the anisotropies of the CMB, lead to a limit of roughly 100 km/s on the possible accuracy of kinetic SZ velocity measurements. This is much higher than what would be expected from considerations of the background noise levels and the few tens of km/s that arise from the difficulty in choosing the appropriate definition of velocity. More work on simulations could shed significant light on optimal strategies for estimating the

true peculiar velocity as well as provide a much better estimate of the distribution of errors that could be expected from an ensemble of galaxy cluster peculiar velocity measurements.

Measurements at cm and mm wavelengths are opening a new window on cosmology. It will soon be possible to measure gas temperatures and peculiar velocities to good accuracy out to $z \sim 2$, allowing unprecedented tests of structure formation as well as an excellent understanding of the topography of much of the observable universe.

I would like to thank Gus Evrard for generously providing access to his simulations and for useful comments and clarifications. This work has benefitted greatly from discussions with, and encouragement from, Arthur Kosowsky, Erik Reese and Lloyd Knox. GPH is supported by the W. M. Keck Foundation.

REFERENCES

Birkinshaw, M. 1999, Physics Reports, **310**, 97.
 Blain, A. W. 1998, MNRAS, **297**, 502.
 Carlstrom, J. E., Holder, G. P., and Reese, E. D. 2002, ARA&A, **40**, 643–80.
 Challinor, A. and Lasenby, A. 1998, ApJ, **499**, 1.
 Dolgov, A. D., Hansen, S. H., Pastor, S., and Semikoz, D. V. 2001, ApJ, **554**, 74.
 Dore, O., Knox, L., and Peel, A. 2002, ApJ, **submitted**, astro-ph/0207369.
 Evrard, A. E. 1988, MNRAS, **235**, 911.
 Haehnelt, M. G. and Tegmark, M. 1996, MNRAS, **279**, 545.
 Hansen, S. H., Pastor, S., & Semikoz, D. V. 2002, ApJ, 573, L69.
 Holder, G. P., Mohr, J. J., Carlstrom, J. E., E., E. A., and Leitch, E. M. 2000, ApJ, **544**, 629.
 Itoh, N., Kohyama, Y., and Nozawa, S. 1998, ApJ, **502**, 7.
 Mathiesen, B. F. and Evrard, A. E. 2001, ApJ, **546**, 100–116.
 Mohr, J. and Evrard, A. 1997, ApJ, **491**, 38.
 Mohr, J., Mathiesen, B., and Evrard, A. 1999, ApJ, **517**, 627.
 Molnar, S. M. and Birkinshaw, M. 1999, ApJ, **523**, 78.
 Nagai, D., Kravtsov, A. V., and Kosowsky, A. 2002, ApJ, **submitted**, astro-ph/0208308.
 Nozawa, S., Itoh, N., and Kohyama, Y. 1998, ApJ, **508**, 17.
 Rephaeli, Y. 1995, ARA&A, **33**, 541.
 Sazonov, S. Y. and Sunyaev, R. A. 1998, ApJ, **508**, 1.
 Seljak, U. and Zaldarriaga, M. 1996, ApJ, **469**, 437–+.
 Sunyaev, R. A. and Zel'dovich, Y. B. 1972, Comments Astrophys. Space Phys., **4**, 173.
 Sunyaev, R. A. and Zel'dovich, Y. B. 1980, ARA&A, **18**, 537.